



Implementing a universal tip asymptotic solution into an Implicit Level Set Algorithm (ILSA) for multiple parallel hydraulic fractures

Dontsov, E.V.¹ and Peirce, A.P.²

¹*University of Houston, Houston, TX, USA*

²*University of British Columbia, Vancouver, BC, Canada*

Copyright 2016 ARMA, American Rock Mechanics Association

This paper was prepared for presentation at the 50th US Rock Mechanics / Geomechanics Symposium held in Houston, Texas, USA, 26-29 June 2016. This paper was selected for presentation at the symposium by an ARMA Technical Program Committee based on a technical and critical review of the paper by a minimum of two technical reviewers. The material, as presented, does not necessarily reflect any position of ARMA, its officers, or members. Electronic reproduction, distribution, or storage of any part of this paper for commercial purposes without the written consent of ARMA is prohibited. Permission to reproduce in print is restricted to an abstract of not more than 200 words; illustrations may not be copied. The abstract must contain conspicuous acknowledgement of where and by whom the paper was presented.

ABSTRACT: The near-tip behavior of a hydraulic fracture determines the local dynamics of the fracture front, and therefore affects the global fracture geometry. Several physical mechanisms may compete to determine the near-tip behavior. In this paper, we consider the simultaneous interplay of fracture toughness, fluid viscosity, and leak-off, which together cause the solution to vary at multiple scales in the near-tip region. In order to avoid having a mesh size that is able to resolve the finest length scale, an Implicit Level Set Algorithm (ILSA), which uses a suitable asymptotic solution for the tip element to locate a fracture front, is employed. The latter asymptotic solution comes from the analysis of a semi-infinite fracture propagating steadily under plane strain elastic conditions. Equipped with an accurate closed-form approximation for this asymptotic solution, which resolves the effects of the fracture toughness, fluid viscosity, and leak-off at all length scales, we analyze the problem of the simultaneous propagation of multiple parallel hydraulic fractures.

1. INTRODUCTION

Hydraulic fracturing is a process, in which a pressurized fluid is injected into a rock formation to induce crack propagation. This technology is used primarily to stimulate oil and gas wells [1], but, in addition, is used for waste disposal [2], rock mining [3], as well as for CO_2 sequestration and geothermal energy extraction [4]. To increase the efficiency of operation in petroleum applications, multiple hydraulic fractures from different perforations are often generated simultaneously from one wellbore. In this situation, outer fractures induce an additional compressive stresses on inner fractures and cause non-uniform fracture growth. This phenomenon is called stress shadowing and has been addressed in numerous studies [5, 6, 7, 8, 9, 10, 11, 12, 13, 14] to name a few. It can significantly affect the fracture geometry and the associated production rate. For this reason, it is important to develop numerical models that are able to predict simultaneous growth of multiple hydraulic fractures and that can be used to design more efficient hydraulic fracture stimulations.

Recognizing the significance of the stress shadowing,

numerous numerical simulators that are able to capture the interaction between multiple hydraulic fractures have been developed such as [5, 8, 9, 11]. Various approximations are used in different simulators, which leads to different accuracy levels and computational times. As shown in numerous studies [15, 16, 17, 18], hydraulic fractures obey a complex multiscale behavior near the fracture tip. Since the tip region determines the fracture dynamics, it is essential to capture the appropriate near-tip features in numerical schemes. One possibility to achieve accurate results is to use a very fine mesh near the tip, which is not always computationally efficient. Another possibility is to incorporate the multiscale tip asymptotic solution into a numerical scheme. In the context of hydraulic fracture modeling, such multiscale features are often not included due to the complexity of tip asymptotic solutions. In contrast, the study [19] implements a multiscale asymptotic solution into a hydraulic fracturing simulator. The aforementioned study considers single planar fracture and captures multiscale tip behavior assuming no leak-off. In terms of predicting multiple fracture growth, the multiscale tip asymptotics has never been used in a hydraulic fracturing simulator.

This study aims to include multiscale tip asymptotic behavior into an Implicit Level Set Algorithm (ILSA) for multiple parallel hydraulic fractures. This is made possible by the recent study [18], in which a closed form approximation for the tip asymptotic solution is derived. This asymptotic solution accounts for simultaneous effects of fracture toughness, fluid viscosity, and fluid leak-off into the formation, and resolves the multiscale behavior. As shown in [18], the error of this approximation is within a small fraction of a percent, which is sufficient for numerical calculations. In contrast to [19], where the leak-off is not included, the universal tip asymptote obtained in [18] is also able to capture fluid leak-off. This opens a possibility to analyze the effect of leak-off on interaction between multiple fractures.

2. MATHEMATICAL MODEL

2.1. ASSUMPTIONS

To formulate the mathematical model for describing the simultaneous growth of multiple parallel hydraulic fractures, it is first necessary to outline a list of assumptions that are used in the model. In particular, it is assumed that:

- All the fractures are planar and perpendicular to the wellbore, see Fig. 1. Five fractures are considered in this paper, but the methodology can be easily extended to any number of fractures.
- Linear elastic fracture mechanics (LEFM) applies for describing the fracture growth, see e.g. [20].
- The rock is linearly elastic and poroelastic effects are ignored.

- The fluid flow is laminar and the fluid is assumed to be incompressible and Newtonian with the dynamic viscosity μ .
- The leak-off is described by Carter's model [21], which assumes a one-dimensional diffusion in the direction perpendicular to the fracture surface, and is quantified by the leak-off coefficient C_L .
- The rock is homogeneous (i.e. the fracture toughness K_{Ic} , Young's modulus E , Poisson's ratio ν , and leak-off coefficient C_L all have uniform values).
- All fractures are always in limit equilibrium, in which case the stress intensity factor is always equal to the fracture toughness at the crack tip.
- The effect of gravity is neglected.
- The fluid front coincides with the crack front, since the lag between the two fronts is negligible under typical high confinement conditions encountered in reservoir stimulation [22, 23].
- The effect of perforation friction is not considered.
- The pay zone layer with height H is surrounded by two other layers, in which an additional compressive stress $\Delta\sigma$ is applied, see Fig. 1. Only two symmetric stress barriers are considered in this study for the purpose of numerical examples. The approach can be extended to arbitrary spatial variation of the compressive stresses. Note that the all layers have the same elastic constants. Capturing spatial variation of elastic properties requires substantial modification of the algorithm that is used in this study.

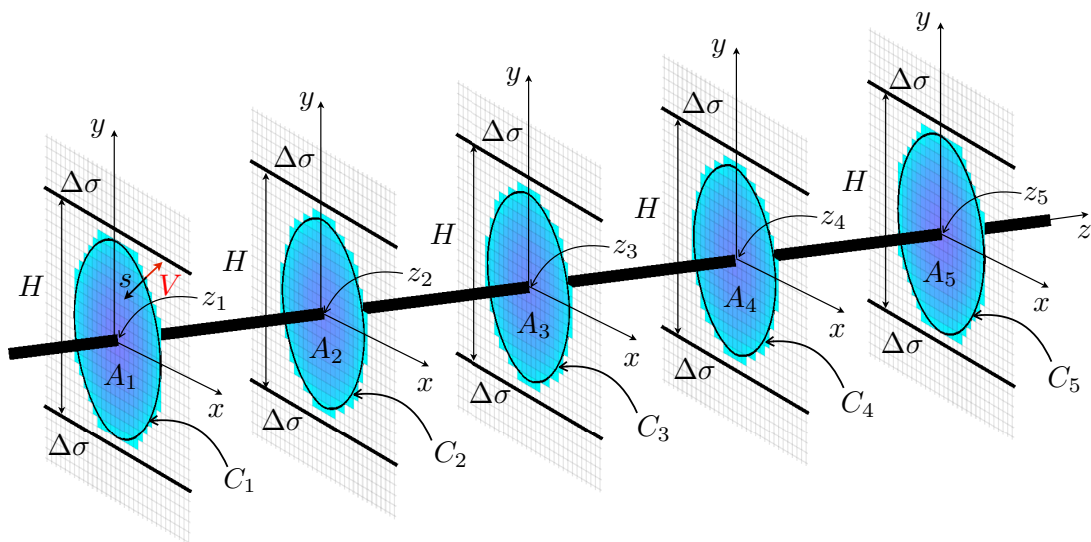


Figure 1: Schematics of simultaneously growing multiple parallel hydraulic fractures.

2.2. GOVERNING EQUATIONS

This section outlines the governing equations for multiple parallel hydraulic fractures. With the reference to Fig. 1, it is noted that the z coordinate lies along the wellbore, while each fracture is contained in the (x, y) plane. The source (wellbore) with total volumetric injection rate $Q(t)$ is located at the origin of each (x, y) plane that contains a fracture, i.e. $(0, 0, z_l)$, where z_l is the location of the perforation and $l = 1 \dots n_p$ is the fracture number ($n_p = 5$ is the total number of fractures). In this setting, the primary quantities of interest in a hydraulic fracture problem are the time histories of the fracture displacement discontinuity components $D_{j,l}(x, y, t)$ $j = 1, 2, 3$, the fluid pressure $p_l(x, y, t)$, the fluid flux entering each fracture $Q_l(t)$, and the position of the front $C_l(t)$. Here $l = 1 \dots n_p$, in which case all the above quantities are calculated for each hydraulic fracture. The fracture width is determined from the displacement discontinuity values as $w_l = D_{z,l}(x, y, t)$. The solution depends on the injection rate $Q(t)$, the far-field compressive stress σ_{zz} , (perpendicular to the fracture planes), and four material parameters μ' , E' , K' , and C' defined as

$$\begin{aligned} \mu' &= 12\mu, & E' &= \frac{E}{1 - \nu^2}, \\ K' &= 4 \left(\frac{2}{\pi} \right)^{1/2} K_{Ic}, & C' &= 2C_L. \end{aligned} \quad (1)$$

Here E' is the plane strain modulus, and μ' is the scaled fluid viscosity, while K' and C' the scaled fracture toughness and leak-off coefficient. Such scaled quantities are introduced to keep equations uncluttered by numerical factors.

2.2.1 Elasticity

Given the rock homogeneity and linear elasticity assumptions, the equations relating the displacement discontinuity component and induced stress fields in the solid can be condensed into the following hypersingular integral equations [24, 25]:

$$\begin{aligned} \sigma_{iz}(x, y, z_k) &= \sum_{l=1}^{n_p} \int_{A_l(t)} C_{izj}(x - \chi, y - \eta, z_k - z_l) \\ &\times D_{j,l}(\chi, \eta) d\chi d\eta, \end{aligned} \quad (2)$$

where $A_l(t)$ denotes the fracture footprint of l th fracture, $C_{izj}(x - \chi, y - \eta, z_k - z_l)$ represents the the iz th stress component at point (x, y, z_k) due to a unit displacement discontinuity at point (χ, η, z_l) in the j th coordinate direction (the expressions for C_{izj} are omitted for brevity). The total stress field is a sum of the hydraulic fracture induced stress whose ij components are σ_{ij} and the geological stress with the ij components σ_{ij}^g . Since the fractures

typically grow in planes that are perpendicular to the minimum principal stress, then $\sigma_{xz}^g(x, y) = \sigma_{yz}^g(x, y) = 0$. To include the effects of stress barriers, the zz component of the geological stress should vary according to

$$\sigma_{zz}^g = \sigma_{zz}^0 + \Delta\sigma \mathcal{H}(y - \frac{1}{2}H) + \Delta\sigma \mathcal{H}(-y - \frac{1}{2}H), \quad (3)$$

where \mathcal{H} denotes Heaviside step function, while H is the thickness of the reservoir layer. Since the fluid cannot sustain shear stresses, the boundary conditions at fracture surfaces are

$$\sigma_{xz}(x, y, z_l) = 0, \quad \sigma_{yz}(x, y, z_l) = 0, \quad (4)$$

while the fluid pressure in l th fracture is calculated based on

$$p_l(x, y) = \sigma_{zz}(x, y, z_l) + \sigma_{zz}^g(x, y), \quad (5)$$

where the expression for the geological stress σ_{zz}^g is given in (3).

2.2.2 Lubrication

Assuming a laminar flow inside the crack, the fluid flux can be calculated based on Poiseuille's law as

$$\mathbf{q}_l = -\frac{w_l^3}{\mu'} \nabla p_l, \quad (6)$$

where $\nabla = (\partial/\partial x, \partial/\partial y)$. The continuity equation for each fracture is

$$\frac{\partial w_l}{\partial t} + \nabla \cdot \mathbf{q}_l + \frac{C'}{\sqrt{t - t_{0,l}(x, y)}} = Q_l(t) \delta(x, y), \quad (7)$$

where the last term on the left hand side captures the fluid leak-off according to the Carter's model, and $t_{0,l}(x, y)$ signifies time instant at which the fracture front of l th fracture was located at the point (x, y) . Equations (6) and (7) can be combined to yield the Reynolds equation for l th fracture

$$\frac{\partial w_l}{\partial t} = \frac{1}{\mu'} \nabla \cdot (w_l^3 \nabla p_l) - \frac{C'}{\sqrt{t - t_{0,l}(x, y)}} + Q_l(t) \delta(x, y), \quad (8)$$

Due to the assumption of no fluid-lag, the governing equation (8) applies within the whole fracture for all $l = 1 \dots n_p$. The fluid fluxes that enter each of the fracture may be different, but the total flux in the wellbore is prescribed, so that

$$\sum_{l=1}^{n_p} Q_l(t) = Q_0(t), \quad p_i(0, 0, t) = p_j(0, 0, t). \quad (9)$$

Here the second equation states that the fluid pressure is the same along the whole wellbore (i.e. for every fracture), while $i = 1 \dots n_p$, $j = 1 \dots n_p$, and $i \neq j$.

2.2.3 Boundary conditions at the moving front

Due to the assumption signifying the applicability of the LEFM solution, the fracture propagation for the mode I crack can be described as [20]

$$\lim_{s \rightarrow 0} \frac{w_l}{s^{1/2}} = \frac{K'}{E'}, \quad (10)$$

where s is the distance to the fracture front. In addition to the propagation condition (10), a zero flux boundary condition at the fracture tip is imposed

$$\lim_{s \rightarrow 0} w_l^3 \frac{\partial p_l}{\partial s} = 0. \quad (11)$$

The evolution of the fracture front $C_l(t)$ (and the associated normal velocity V) is implicitly determined by the equations (2), (8), (10) and (11), which apply for all fractures $l = 1 \dots n_p$.

3. UNIVERSAL TIP ASYMPTOTIC SOLUTION

3.1. THE NEED FOR A MULTISCALE TIP ASYMPTOTIC SOLUTION

Analysis of the near tip behavior of hydraulic fractures indicates that the validity region of the propagation condition (10) is often limited to the immediate vicinity of the tip (see e.g. [17]). In this situation, a very fine mesh is required to accurately resolve the square root behavior near the tip, which, in turn, substantially increases the computational cost. In order to avoid this situation, one can replace the propagation condition (10) by a solution with an increased validity region

$$w(s) \approx w_a(s), \quad s = o(L), \quad (12)$$

where $w_a(s)$ is the fracture width variation in the near tip region, and L is the characteristic length of the fracture. The universal asymptotic solution w_a can be calculated by considering a semi-infinite hydraulic fracture that propagates steadily with the velocity V in plane strain elastic conditions [17, 26].

3.2. PROBLEM FORMULATION AND VERTEX SOLUTIONS

The governing equations for the near tip problem can be written as [17, 18, 26]

$$\begin{aligned} \frac{w_a^2}{\mu'} \frac{dp_a}{ds} &= V + 2C'V^{1/2} \frac{s^{1/2}}{w_a}, \\ p_a(s) &= \frac{E'}{4\pi} \int_0^\infty \frac{dw_a(s')}{ds'} \frac{ds'}{s-s'}, \\ w_a &= \frac{K'}{E'} s^{1/2}, \quad s \rightarrow 0, \end{aligned} \quad (13)$$

where $w_a(s)$ is the fracture width variation away from the tip, p_a is the fluid pressure, V is the fracture propagation velocity, while s is the distance from the fracture tip.

It is important to note that there are three limiting regimes of propagation, namely, toughness (denoted by k), leak-off (denoted by \tilde{m}), and viscous (denoted by m) [17]. The fracture width solutions (so-called vertex solutions) for these regimes are respectively given by

$$\begin{aligned} w_k &= \frac{K'}{E'} s^{1/2}, & w_{\tilde{m}} &= \beta_{\tilde{m}} \left(\frac{4\mu'^2 V C'^2}{E'^2} \right)^{1/8} s^{5/8}, \\ w_m &= \beta_m \left(\frac{\mu' V}{E'} \right)^{1/3} s^{2/3}, \end{aligned} \quad (14)$$

where $\beta_{\tilde{m}} = 4/(15^{1/4}(\sqrt{2}-1)^{1/4})$ and $\beta_m = 2^{1/3}3^{5/6}$. The knowledge of the vertex solutions (14), however, is not sufficient, since they represent only limiting cases. In this case, a different approach should be chosen.

3.3. APPROXIMATE SOLUTION

This study utilizes an approximate closed form solution of (13) that has been obtained in [18]. Following [27], the solution can be written in terms of the dimensionless quantities

$$\hat{K} = \frac{K' s^{1/2}}{E' w_a}, \quad \hat{C} = \frac{2C' s^{1/2}}{V^{1/2} w_a}, \quad \hat{s} = \frac{\mu' V s^2}{E' w_a^3}, \quad (15)$$

where $0 \leq \hat{K} \leq 1$ is related to scaled fracture toughness, $\hat{C} \geq 0$ represents the normalized leak-off, and \hat{s} is the scaled s coordinate. The expression that provides solution implicitly is

$$\begin{aligned} \hat{s} &= \frac{1}{3C_1(\delta)} \left[1 - \hat{K}^3 - \frac{3}{2} \hat{C} \hat{b} (1 - \hat{K}^2) + 3\hat{C}^2 \hat{b}^2 (1 - \hat{K}) \right. \\ &\quad \left. - 3\hat{C}^3 \hat{b}^3 \ln \left(\frac{\hat{C} \hat{b} + 1}{\hat{C} \hat{b} + \hat{K}} \right) \right] \equiv f(\hat{K}, \hat{C} \hat{b}, C_1), \end{aligned} \quad (16)$$

where $\hat{b} = C_2(\delta)/C_1(\delta)$ and

$$\begin{aligned} C_1(\delta) &= \frac{4(1-2\delta)}{\delta(1-\delta)} \tan(\pi\delta), \\ C_2(\delta) &= \frac{16(1-3\delta)}{3\delta(2-3\delta)} \tan\left(\frac{3\pi}{2}\delta\right). \end{aligned} \quad (17)$$

As follows from [18, 27], the zeroth-order approximation can be obtained from (16) as

$$\hat{s} = f\left(\hat{K}, \frac{3\beta_m^4}{4\beta_m^3} \hat{C}, \frac{\beta_m^3}{3}\right) \equiv g_0(\hat{K}, \hat{C}). \quad (18)$$

To calculate a more accurate solution, one should calculate δ as

$$\delta = \frac{\beta_m^3}{3} \left(1 + \frac{3\beta_m^4}{4\beta_m^3} \hat{C} \right) g_0(\hat{K}, \hat{C}) \equiv \Delta(\hat{K}, \hat{C}), \quad (19)$$

and substitute the result into (16) to obtain

$$\hat{s} = f\left(\hat{K}, \hat{C}\hat{b}(\Delta(\hat{K}, \hat{C})), C_1(\Delta(\hat{K}, \hat{C}))\right) \equiv g_\delta(\hat{K}, \hat{C}). \quad (20)$$

The latter equation (20) can be expressed in the dimensional form using (15) as

$$\frac{s^2 V \mu'}{E' w_a^3} = g_\delta\left(\frac{K' s^{1/2}}{E' w_a}, \frac{2 s^{1/2} C'}{w_a V^{1/2}}\right). \quad (21)$$

Equation (21) provides an approximate closed-form implicit solution for the fracture aperture variation in the tip region $w_a(s)$ (12). The latter solution obeys a multiscale behavior, and is able to capture all limiting solutions (14) together with all possible transition regions, see [18, 27] for more details. Note here that g_δ is a relatively simple function, so that a numerical evaluation of the solution through (21) is computationally efficient.

3.4. PARAMETRIC TRIANGLE

To quantify the ‘‘position’’ of the fracture opening solution relative to the vertex solutions (14), it is useful to introduce a concept of a parametric triangle, after [17]. To draw this triangle in a quantitative manner, let us first introduce shape functions associated with the vertex solutions (14), and universal asymptotic solution w_a (21) as

$$\begin{aligned} n_k &= \frac{w_k}{w - w_k}, & n_{\tilde{m}} &= \frac{w_{\tilde{m}}}{w - w_{\tilde{m}}}, \\ n_m &= \frac{w_m}{w - w_m}, \\ N_k &= \frac{n_k}{n_k + n_m + n_{\tilde{m}}}, & N_{\tilde{m}} &= \frac{n_{\tilde{m}}}{n_k + n_m + n_{\tilde{m}}}, \\ N_m &= \frac{n_m}{n_k + n_m + n_{\tilde{m}}}. \end{aligned} \quad (22)$$

By selecting location of the vertices as $(x_m, y_m) = (0, 0)$, $(x_{\tilde{m}}, y_{\tilde{m}}) = (1/2, \sqrt{3}/2)$, and $(x_k, y_k) = (1, 0)$, a point inside the triangle is determined by

$$\begin{aligned} x_{tr} &= x_m N_m + x_{\tilde{m}} N_{\tilde{m}} + x_k N_k, \\ y_{tr} &= y_m N_m + y_{\tilde{m}} N_{\tilde{m}} + y_k N_k. \end{aligned} \quad (23)$$

The colour filling of the triangle is calculated based on the values of the shape functions as $[R, G, B] = [N_k, N_{\tilde{m}}, N_m]$.

4. NUMERICAL RESULTS

This section presents results of the numerical solution of (2)–(5), (8), (9) with the propagation condition (12) that is calculated using the approximate solution (21). The Implicit Level Set Algorithm (ILSA) is used to construct the numerical scheme, see [9, 19, 26, 27] that use a similar approach. The details of the numerical scheme are omitted

for brevity and can be found in [27]. Material parameters that are used in the examples are

$$\begin{aligned} E &= 9.5 \text{ GPa}, & \nu &= 0.2, & \mu &= 0.1 \text{ Pa}\cdot\text{s}, \\ Q_0 &= 0.05 \text{ m}^3/\text{s}, & K_{Ic} &= 1 \text{ MPa}\cdot\text{m}^{1/2}, & H &= 20 \text{ m}. \end{aligned} \quad (24)$$

Three different values of leak-off are considered, namely

$$C' = \{0.521, 1.65, 5.21\} \times 10^{-5} \text{ m/s}^{1/2}, \quad (25)$$

which correspond to a dimensionless leak-off parameter

$$\phi = \frac{\mu'^3 E'^{11} C'^4 Q_0}{K'^{14} n_p} = \{10^{-4}, 10^{-2}, 1\}. \quad (26)$$

The values of the compressive stresses in (3) are chosen as

$$\sigma_{zz}^0 = 7 \text{ MPa}, \quad \Delta\sigma = 0.75 \text{ MPa}. \quad (27)$$

The spacing between perforations is selected to be uniform and equal to 20 m, i.e. $z_{k+1} - z_k = 20 \text{ m}$ for $k = 1 \dots n_p - 1$. This study focuses on the case of five parallel fractures, i.e. $n_p = 5$.

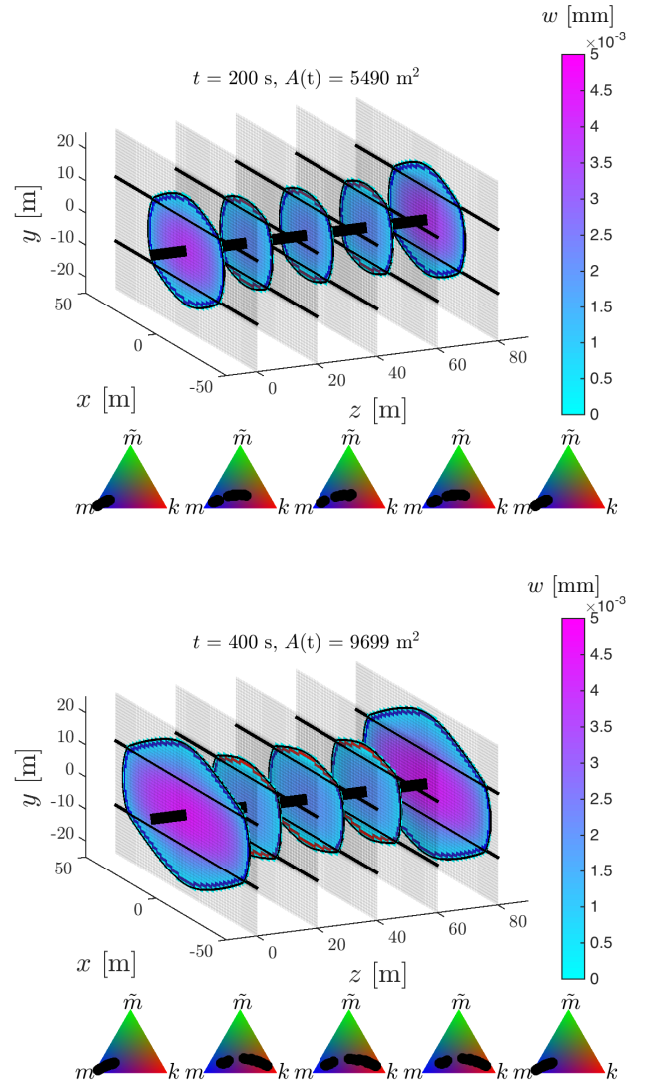


Figure 2: Results of the numerical simulations for $t = 200 \text{ s}$ (top) and $t = 400 \text{ s}$ (bottom) for $\phi = 10^{-4}$.

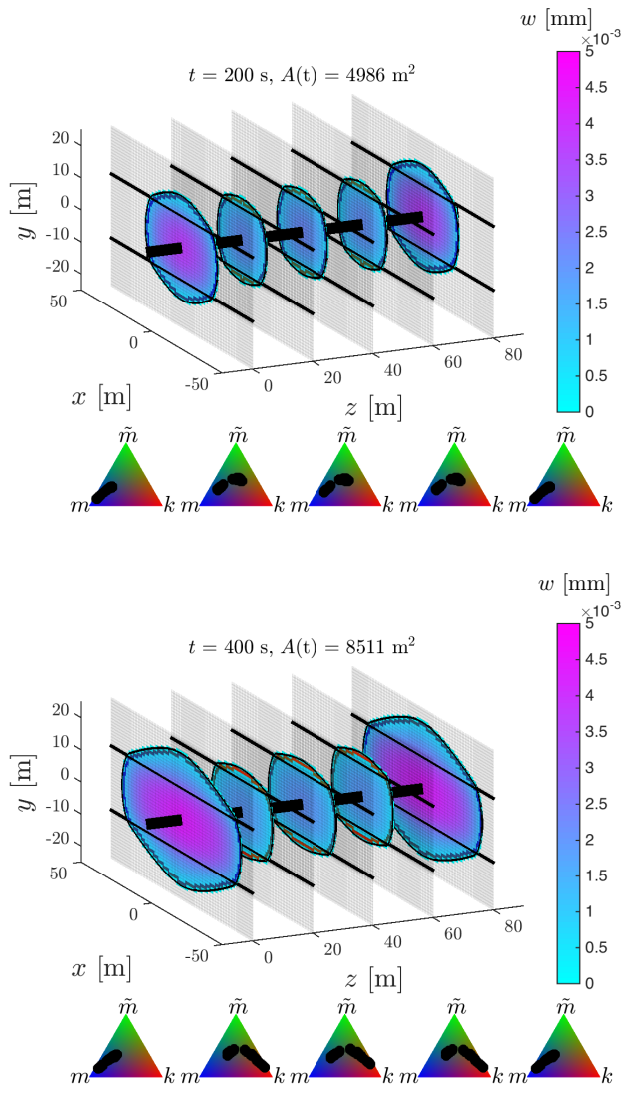


Figure 3: Results of the numerical simulations for $t = 200$ s (top) and $t = 400$ s (bottom) for $\phi = 10^{-2}$.

Figs. 2-4 show the results of the numerical simulations for the three different values of leak-off considered. The top pictures show the results at $t = 200$ s, while the bottom pictures show the solution for $t = 400$ s. Color filling indicates the fracture width according to the colorbar. The fracture boundaries (footprints) are highlighted by solid black lines, locations of the stress barriers are shown by thicker solid lines (at $y = 10$ m and $y = -10$ m), while the thickest black line passing through $x = 0, y = 0$ schematically indicates the wellbore. The total surface area, $A(t)$, of all five fractures at time t is shown on each picture. Elements that are used to locate moving fracture front are called survey elements and have a special color filling. The color of each element corresponds to the asymptotic solution that is used in this element to locate the front, see Section (3.4) for the description. Five parametric triangles (see Section (3.4)) below each picture indicate the location of the asymptotic solutions that are used in survey elements. The left-most triangle corresponds to the

left-most fracture ($z = 0$ plane), the right-most triangle corresponds to the right-most fracture ($z = 80$ m plane), while the intermediate triangles represent three intermediate fracture planes. From Fig. 2, we can observe that the outer fractures use the m vertex solution at $t = 200$ s, while the inner fractures utilize the asymptotic solutions that are located inside the triangle. This shows that the outer fractures propagate faster than the inner ones due to stress shadowing. The trend becomes more apparent for $t = 400$ s, which shows that the outer fractures are substantially larger in size. Similar stress shadowing effect is produced for larger leak-off values, as can be seen in Figs. 3 and 4. The primary differences are the fracture dimensions and the asymptotic solutions that are used in the survey elements. Note the variability of the asymptotic solutions that are used in all the results. This highlights the necessity of using the universal asymptotic solution to capture the large range of length scales active in the problem.

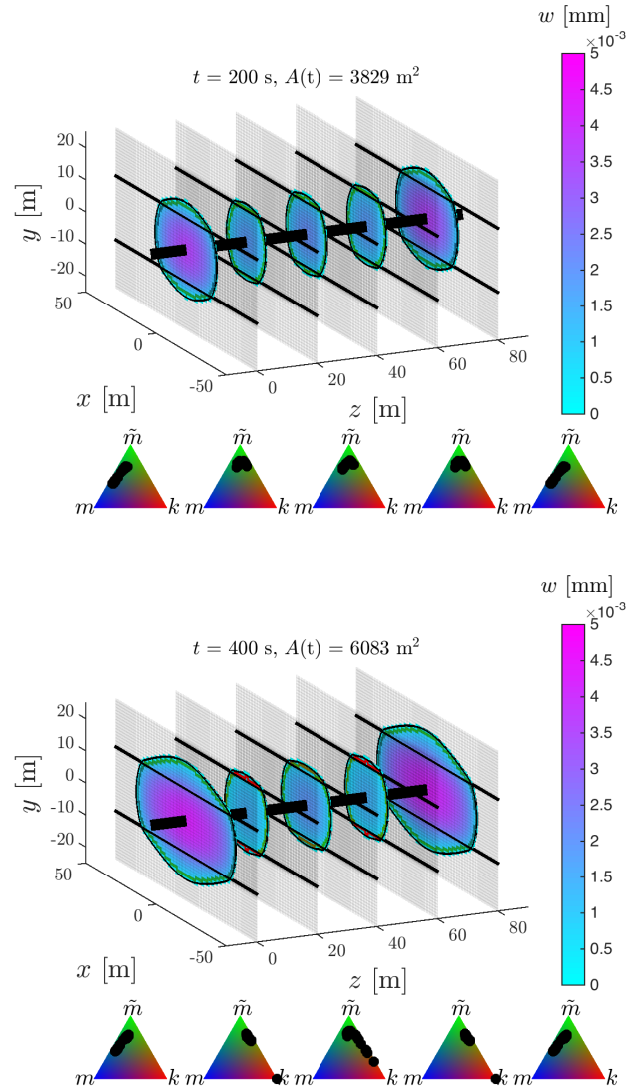


Figure 4: Results of the numerical simulations for $t = 200$ s (top) and $t = 400$ s (bottom) for $\phi = 1$.

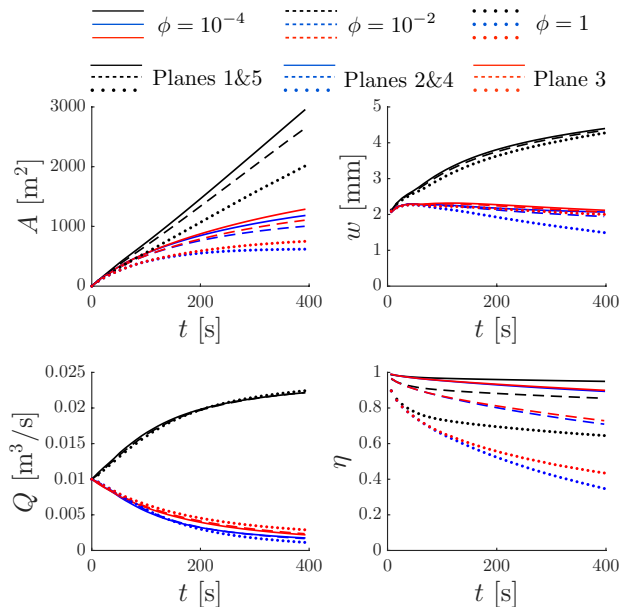


Figure 5: Time histories of fracture area (top left), width at the wellbore (top right), flux (bottom left), and efficiency (bottom right) for all fracture planes and $\phi = \{10^{-4}, 10^{-2}, 1\}$.

To quantify the effect of leak-off on the propagation of multiple hydraulic fractures, Fig. 5 shows the time histories of the fracture area (top left), the fracture width at the wellbore, i.e. at $x = 0$ and $y = 0$ (top right), the fluid flux (bottom left), and the efficiency (bottom right) for every fracture and different values of the leak-off parameter. Here the efficiency is defined as the ratio between current fracture volume and the total amount fluid that has been pumped into it. Results for planes 1 and 5 (located at $z = 0$ and $z = 80$ m) are identical due to symmetry and are indicated by black lines. Results for planes 2 and 4 (located at $z = 20$ and $z = 60$ m) are also identical due to symmetry and are indicated by blue lines. Results for the middle plane 3 (located at $z = 40$ m) are indicated by red lines. The results that correspond to $\phi = 10^{-4}$ are indicated by solid lines, $\phi = 10^{-2}$ results are shown by dashed lines, while $\phi = 1$ results are indicated by dotted lines. In all cases, the outer fractures consume most of the fluid due to stress shadowing. The value of the fluid flux for the outer fractures is almost independent of leak-off, while the fluxes for inner fractures change for large leak-off case $\phi = 1$. The efficiency, on the other hand, strongly depends on leak-off and inner fractures are noticeably less efficient than the outer fractures. The fracture areas depend on both the flux distribution and leak-off and their ratios are a direct consequence of the flux distribution. It is interesting to observe that the wellbore width of the inner fractures starts to decrease at some point due to additional compressive stresses produced by the outer fractures. This feature becomes especially pronounced for large leak-off case $\phi = 1$ for planes 2 and 4. Such dynamics may poten-

tially lead to fracture closing, which is very undesirable in practical applications.

5. SUMMARY

The primary goal of this paper is to describe a procedure for implementing a universal tip asymptotic solution into the hydraulic fracturing simulator ILSA [9, 19, 26, 27] that is able to model simultaneous growth and interaction of multiple parallel hydraulic fractures. Firstly, the governing equations that are utilized by the numerical simulator are outlined. Then, a closed form approximation for multiscale tip asymptotic solution, which is used to locate moving fracture front, is presented. This solution accounts for a simultaneous interplay between fracture toughness, fluid viscosity, and leak-off, which together cause the multiscale behavior. The growth of 5 parallel fractures is considered. To understand the effect of leak-off, three different values of leak-off are selected. Results demonstrate that the leak-off does not significantly affect the flux in outer fractures (for the examples considered), but, at the same time, may affect inner fractures, changes fracture growth dynamics, efficiency, and promotes stress shadowing by reducing the efficiency of the inner “shadowed” fractures.

ACKNOWLEDGEMENTS

Authors would like to acknowledge the support of the British Columbia Oil and Gas Commission and the NSERC discovery grants program.

REFERENCES

1. Economides, M.J. and K.G. Nolte, editors. *Reservoir Stimulation*. John Wiley & Sons, Chichester, UK, 3rd edition, 2000.
2. Abou-Sayed, A.S., D.E. Andrews, and I.M. Buhidma. Evaluation of oily waste injection below the permafrost in Prudhoe Bay field. In *Proceedings of the California Regional Meetings, Bakersfield, CA, Society of Petroleum Engineers*, pages 129–142, 1989.
3. Jeffrey, R.G. and K.W. Mills. Hydraulic fracturing applied to inducing longwall coal mine goaf falls. In *Pacific Rocks 2000, Balkema, Rotterdam*, pages 423–430, 2000.
4. Brown, D.W. . A hot dry rock geothermal energy concept utilizing supercritical CO_2 instead of water. In *Proceedings of Twenty-Fifth Workshop on Geothermal Reservoir Engineering Stanford University, Stanford, California*, 2000.

5. Olson, J.E. Multi-fracture propagation modeling: Applications to hydraulic fracturing in shales and tight gas sands. In *In Proceedings 42nd U.S. Rock Mechanics Symposium. San Francisco, CA, USA*, 2008.
6. Singh, I. and J.L. Miskimins. A numerical study of the effects of packer-induced stresses and stress shadowing on fracture initiation and stimulation of horizontal wells. In *Proceedings of the Canadian Unconventional Resources & International Petroleum Conference, CSUG/SPE 136856*, 2010.
7. McClure, M.W. and M.D. Zoback. Computational investigation of trends in initial shut-in pressure during multi-stage hydraulic stimulation in the barnett shale. In *In Proceedings 47nd U.S. Rock Mechanics Symposium. San Francisco, CA, USA*, 2013.
8. Kresse, O., X. Weng, H. Gu, and R. Wu. Numerical modeling of hydraulic fracture interaction in complex naturally fractured formations. *Rock Mech. Rock Eng.*, 46:555–558, 2013.
9. Peirce, A.P. and A.P. Bunger. Interference fracturing: Non-uniform distributions of perforation clusters that promote simultaneous growth of multiple hydraulic fractures. *SPE 172500*, 2014.
10. Daneshy, A. Fracture shadowing: Theory, applications and implications. In *Proceedings of the SPE Annual Technical Conference and Exhibition, SPE-170611-MS*, 2014.
11. Wu, K., J. Olson, M.T. Balhoff, and W. Yu. Numerical analysis for promoting uniform development of simultaneous multiple fracture propagation in horizontal wells. In *Proceedings of the SPE Annual Technical Conference and Exhibition, SPE-174869-MS*, 2015.
12. Skomorowski, N., M.B. Dussealut, and R. Gracie. The use of multistage hydraulic fracture data to identify stress shadow effects. In *In Proceedings 49nd U.S. Rock Mechanics Symposium. San Francisco, CA, USA*, 2015.
13. Kumar, D. and A. Ghassemi. 3D simulation of multiple fracture propagation from horizontal wells. In *In Proceedings 49nd U.S. Rock Mechanics Symposium. San Francisco, CA, USA*, 2015.
14. Manchanda, R., E.C. Bryant, P. Bhardwaj, P. Cardiff, and M.M. Sharma. Strategies for effective stimulation of multiple perforation clusters in horizontal wells. In *Proceedings of the SPE Hydraulic Fracturing Technology Conference, SPE-179126-MS*, 2016.
15. Desroches, J., E. Detournay, B. Lenoach, P. Papanastasiou, J.R.A. Pearson, M. Thiercelin, and A.H.-D. Cheng. The crack tip region in hydraulic fracturing. *Proc. R. Soc. Lond. A*, 447:39–48, 1994.
16. Detournay, E.. Propagation regimes of fluid-driven fractures in impermeable rocks. *Int. J. Geomech.*, 4:35–45, 2004.
17. Garagash, D.I., E. Detournay, and J.I. Adachi. Multi-scale tip asymptotics in hydraulic fracture with leak-off. *J. Fluid Mech.*, 669:260–297, 2011.
18. Dontsov, E.V. and A.P. Peirce. A non-singular integral equation formulation to analyze multiscale behaviour in semi-infinite hydraulic fractures. *J. Fluid. Mech.*, 781:R1, 2015.
19. Peirce, A.P. Modeling multi-scale processes in hydraulic fracture propagation using the implicit level set algorithm. *Comp. Meth. in Appl. Mech. and Eng.*, 283:881–908, 2015.
20. Rice, J.R. Mathematical analysis in the mechanics of fracture. In H. Liebowitz, editor, *Fracture: An Advanced Treatise*, volume II, chapter 3, pages 191–311. Academic Press, New York, NY, 1968.
21. Carter, E.D. Optimum fluid characteristics for fracture extension. In *Howard GC, Fast CR, editors. Drilling and production practices*, pages 261–270, 1957.
22. Garagash, D. and E. Detournay. The tip region of a fluid-driven fracture in an elastic medium. *J. Appl. Mech.*, 67:183–192, 2000.
23. Detournay, E. and A. Peirce. On the moving boundary conditions for a hydraulic fracture. *Int. J. Eng. Sci.*, 84:147–155, 2014.
24. Crouch, S.L. and A.M. Starfield. *Boundary Element Methods in Solid Mechanics*. George Allen and Unwin, London, 1983.
25. Hills, D.A., P.A. Kelly, D.N. Dai, and A.M. Korsunsky. *Solution of crack problems, The Distributed Dislocation Technique, Solid Mechanics and its Applications*, volume 44. Kluwer Academic Publisher, Dordrecht, 1996.
26. Peirce, A. and E. Detournay. An implicit level set method for modeling hydraulically driven fractures. *Comput. Methods Appl. Mech. Engrg.*, 197:2858–2885, 2008.
27. Dontsov, E.V. and A.P. Peirce. A multiscale Implicit Level Set Algorithm (ILSA) to model hydraulic fracture propagation incorporating combined viscous, toughness, and leak-off asymptotics. *In preparation*, 2016.